Optical Materials 34 (2011) 207–214

Contents lists available at SciVerse ScienceDirect

Optical Materials

journal homepage: www.elsevier.com/locate/optmat

Surface ablation of $RbTiOPO_4$ by femtosecond laser

G. Raj Kumar [a], J.J. Carvajal [a,*], M.C. Pujol [a], X. Mateos [a], J. Grau [b], J. Massons [a], J.R. Vázquez de Aldana [c], C. Méndez [d], P. Moreno [c], L. Roso [d], J. Ferré-Borrull [e], J. Pallarès [e], L.F. Marsal [e], M. Aguiló [a], F. Díaz [a]

[a] Física i Cristal·lografia de Materials i Nanomaterials (FiCMA-FiCNA), Universitat Rovira i Virgili (URV), Campus Sescelades, Marcel·li Domingo, s/n Tarragona E-43007, Spain
[b] EUETIB, Univ. Politècnica de Catalunya (UPC), Barcelona, Spain
[c] Grupo de Microprocesado de Materiales con Láser, Univ. Salamanca, Salamanca E-37008, Spain
[d] CLPU-Centro de Láseres Pulsados, Villamayor, Salamanca E-37185, Spain
[e] Dept. d'Enginyeria Electrònica, Univ. Rovira i Virgili (URV), Tarragona E-43007, Spain

ARTICLE INFO

Article history:
Received 5 May 2011
Received in revised form 29 July 2011
Accepted 11 August 2011
Available online 9 September 2011

Keywords:
Non-linear optical materials
Ultrafast laser ablation

ABSTRACT

We report here the results obtained in surface ablation of $RbTiOPO_4$ single crystals by femtosecond laser. We fabricated and characterized one-dimensional (1D) diffraction gratings with different lattice spacings of 15 and 20 μm, and with a sub-modulation of the period introduced in the later. The optical and electronic microscopy characterization and filling factor analysis of these diffraction gratings are reported. We also show that the roughness generated on the grooves by the ablation process can be improved by chemical etching.

1. Introduction

Second harmonic generation (SHG) of laser radiation by phase matching (PM) in non-centrosymmetric crystals is commonly used for the generation of coherent sources of short-wavelength radiation. For non-linear crystals where direct phase matching is not possible, phase-matching conditions for processes such as second harmonic generation (SHG) can be fulfilled by periodically modulating the material. The periodicity of any physical property of the material introduces reciprocal lattice vectors that provide the phase matching conditions between the incident and the generated beam, a mechanism called quasi-phase matching (QPM) [1,2]. A very common means to achieve QPM is by periodic poling of non-linear material, in which case only the χ^2 tensor shows a periodic modulation, while the refractive index has no modulation whatsoever. However, if other patterning methods are employed, a modulation of the refractive index of the material, for instance, can be achieved. Such periodically modulated materials can be used to generate a non-linear optical response, even in centrosymmetric materials [3]. More interestingly, SHG in these structures may be generated through a non-collinear configuration that can provide several advantages when compared to the more conventional collinear QPM configuration, such as the automatic separation of the generated beam from the input beam [4].

$RbTiOPO_4$ (RTP) is a non-linear optical material that belongs to the family of the well known $KTiOPO_4$ (KTP). KTP is one of the materials of reference for the fabrication of solid state lasers emitting in the green region of the electromagnetic spectrum by second harmonic generation of Nd:YAG lasers [5]. RTP has, however, the advantages to respect KTP, that while presenting similar non-linear optical coefficients [6], it shows larger electro-optic coefficients [7], and a higher damage threshold than KTP [8], which makes it specially attractive for electro-optics applications.

We structured the surface of RTP single crystals by ultrafast laser ablation, forming one-dimensional (1D) surface-relief diffraction gratings. In these structures, the refractive index and the non-linear optical response of the material are periodically modulated at its surface. Such structures might have interest for the analysis of non-linear optical effects, since in these structures not only the QPM conditions can be fulfilled in the case of an external beam incident on the surface of the diffraction grating from the top half-space, but also, both the fundamental and the SH fields can be strongly localized via resonant Bloch modes of the periodic structure [9–11].

Ultrafast laser ablation is a low cost technique that provides fast procedures and one step processing. Femtosecond infrared laser pulses have been successfully applied to the micro-structuring of dielectric transparent crystals and glasses. Such pulses are focused in the material, leading to laser ablation of the exposed area with minimal mechanical and thermal deformation for the rest of the material [12]. This technique has been already used to structuring non-linear optical materials such as KH_2PO_4 (KDP) [13], $LiNbO_3$ [14], β-BaB_2O_4 (BBO) [15,16], and $LiTaO_3$ [17].

* Corresponding author. Tel.: +34 977 55 8790; fax: +34 977 55 9563.
E-mail address: joanjosep.carvajal@urv.cat (J.J. Carvajal).

0925-3467/$ - see front matter © 2011 Elsevier B.V. All rights reserved.
doi:10.1016/j.optmat.2011.08.007

In this paper, we analyze the results obtained in the structuring of the (001) surface of RTP single crystals with a femtosecond laser system forming two diffraction gratings with different grating spacings. We characterized morphologically these diffraction gratings by optical and electronic microscopy and analyzed their diffractive properties. We also smoothed the roughness generated during the ablation process by applying a chemical etching technique.

2. Experimental techniques

2.1. Crystal growth

RTP is an orthorhombic material crystallizing with the $Pna2_1$ space group of symmetry [17]. RTP melts incongruently at 1443 K [18], so it cannot be grown from its melt. The Top-Seeded Solution Growth (TSSG) technique is one of the techniques included in the high temperature solution (HTS) growth techniques. One of the advantages of crystal growth from high temperature solutions (or flux growth), is that it allows crystals to grow below their melting temperature. A vertical tubular furnace, controlled by a Eurotherm 903 controller/programmer and a platinum cylindrical crucible of 125 cm^3 has been used in the crystal growth experiments. The solution was prepared by mixing the corresponding ratios of the precursor oxides, Rb_2CO_3, TiO_2, and P_2O_5. RTP crystals were grown from WO_3 containing fluxes to reduce the viscosity of the flux and to overcome the difficulty for the structural units to reach the crystal solution interface [19]. The composition of the solution used to grow these RTP crystals was Rb_2O–TiO_2–P_2O_5–WO_3 = 42.24–16.80–18.96–20.00 mol%. A ***c***-oriented crystal seed was used for growing RTP crystals and also for the determination of saturation temperature by examining the growth or dissolution of the crystalline seed in contact with the solution surface. In all these cases, the crystal seed was placed on the surface of the solution, just in the centre of the platinum crucible. A crystal seed rotation was maintained in all cases at an angular speed of 45 rpm to favor a good homogenization of the growth solution, and avoid the formation of flux inclusions in the crystals. During the crystal growth process, the temperature was reduced by 20–30 K, depending on the size of the desired crystal, from the saturation temperature at a rate of 0.1 K/h. To obtain larger crystals, the as-growing crystals were pulled out very slowly from the solution at a rate of 0.5 mm every 12 h. Finally, when the crystal growth process was finished, the crystal was slowly extracted from the solution and slowly cooled to room temperature inside of the furnace to avoid thermal stresses that can result in cracks in the crystals.

The samples, on which the surface relief diffraction gratings were fabricated, were prepared from the single crystals obtained, by cutting and polishing them in a crystallographically oriented way. First, samples were cut with the correct crystallographic orientation to obtain surface perpendicular to the ***c***-crystallographic direction, using a goniometer coupled to a Struers Accutom-50 diamond saw with disks 0.12 mm thick. Later the samples were polished in a Logitech PM5 polisher with an oscillatory arm. This enabled accurately rotation and pressurization of the samples, depending on the hardness of the material to be polished. As abrasive substances, alumina powders of 9, 3, 1 and 0.3 μm diameters were used. The quality of the polishing was measured using parameters such as roughness, flatness and parallelism between opposite faces of the sample measured by a Sensofar PLμ 2300 interferometric confocal microscope and a home-made self–collimator.

2.2. Ultrafast laser ablation

We used a commercial Ti: Sapphire Oscillator (Tsunami, Spectra Physics) and a regenerative amplifier system (Spitfire, Spectra Physics) based on chirped pulsed amplification (CPA) for ultrafast laser ablation of the surface of RTP samples. The system delivers linearly polarized pulses of duration 120 fs at 795 nm with a repetition rate of 1 kHz. The maximum pulse energy is 1 mJ and it was reduced by means of neutral density filters and a combination of a half wavelength plate and linear polarizer in order to micro-structure the gratings with the required geometry. The transversal mode is Gaussian and beam diameter is 9 mm ($1/e^2$ criterion). Before recording the gratings, we have estimated the ablation threshold fluence for RTP following the procedure proposed by Dumitru and co-workers [21]. The threshold fluence depends on the number of pulses per spot, resulting 1.44 ± 0.18 J cm^{-2} for 40 pulses and decreasing to 1.18 ± 0.15 J cm^{-2} for multi shot conditions (>100 pulses). The value of the incubation factor was calculated, giving $\xi = 0.783$ [21].

Processing parameters were chosen to record one grating with spatial period (Λ) of 15 μm (grating RTP1) and another grating with $\Lambda = 20$ μm (grating RTP2). For recording RTP1, the pulse energy was 0.78 μJ. The laser pulses were focused by means of a 50 mm achromatic lens which provided a peak fluence of $\sim$6.1 J cm^{-2} at focus. The sample, which was 2 mm thick, was placed on a motorized XYZ translation stage that allowed achieving optimal focusing on the surface of the target, with the (001) face of the samples perpendicular to the laser beam. The sample was moved following straight lines parallel to the ***b*** crystallographic axis and all across the surface, at a constant scanning speed of 130 μm s^{-1} avoiding iterative passes along the same line. The pitch between the lines was set to 15 μm. For that scanning speed and focusing conditions the number of pulses contributing to the ablation of a point within the sample surface was approximately 40.

For recording RTP2, the focusing optics was a 10X (0.22 NA) microscope objective. A 6 mm diameter circular aperture was placed before the objective in order to slightly increase the spot size at focus. The pulse energy before the aperture was set to 0.27 μJ leading to peak fluence at focus of $\sim$3.2 J cm^{-2}. The writing procedure was identical than for RTP1 but now the scanning speed was set to 75 μm s^{-1} and the separation between lines was 10.5 μm and 9.5 μm alternatively. Under these conditions, the number of pulses contributing to the ablation of a point within the sample surface was around 55.

2.3. Chemical etching

Chemical etching is one of the simplest and widely applied techniques to observe ferroelectric domain structures in crystals of the KTP family. In particular molten KOH:KNO_3 mixtures have been extensively studied for this purpose in this family of materials. Here, we used this selective chemical etchant, that etches the negative (001) face of the crystal while the positive (001) face is left relatively unetched, to smooth the roughness generated by the ultrafast laser ablation process. We performed the chemical etching process by dissolving a mixture of KOH:KNO_3 2:1 M ratio in distilled water at 353 K, and immersed the diffraction gratings between 5 min and 1 h in this solution. After that, the diffraction gratings were observed again under the Scanning Electron Microscope to record the effects generated on the grooves of the diffraction gratings by this chemical etching process.

3. Results and discussion

3.1. Crystal growth of RTP single crystals

RTP single crystals with typical dimensions of 17 × 18 × 20 mm along the ***a*** × ***b*** × ***c*** crystallographic directions and a typical weight of 9.3 g were obtained from high-temperature solutions containing

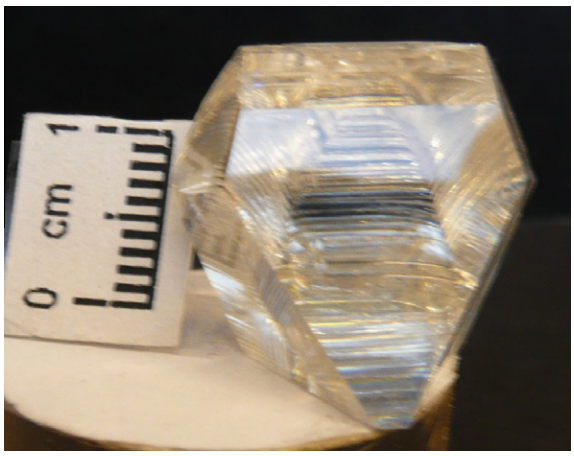

Fig. 1. $RbTiOPO_4$ single crystal obtained by Top-Seeded Solution Growth associated to a slow cooling of the solution. Pulling of the crystal from the solution was used to get a bigger crystal.

20 mol% WO_3. Fig. 1 shows an as-grown RTP single crystal. Tungsten oxide was used to decrease the viscosity of the solution of growth, that otherwise has been reported to be very high in this family of materials [22]. The composition of the solution of growth was chosen to be inside the crystallization region of RTP when a 20 mol% WO_3 was introduced in the solution [20]. The crystals were obtained by decreasing by 20–30 K the temperature of the solution starting from the saturation temperature, that was determined to be 910 K. This temperature is lower than the Curie temperature determined for these crystals, that has been determined to be 1065 K by measuring the dielectric permittivity of the crystal as a function of the temperature. This Curie temperature is lower than that measured for RTP crystals grown in solutions not containing WO_3 [23].

From these single crystals, slabs with typical dimensions $4 \times 4 \times 3$ mm along the $\boldsymbol{a} \times \boldsymbol{b} \times \boldsymbol{c}$ crystallographic axes were cut and their six faces polished to optical quality. On the (001) face of these samples is were laser ablation was performed.

3.2. Micro-structure analysis of the as fabricated diffraction gratings

The as-fabricated diffraction gratings were observed by optical microscopy. From this analysis, a long range order was observed indicating a high degree of periodicity of the two RTP samples, as can be seen in Fig. 2a and b for RTP1 and RTP2 samples, respectively.

From these figures it can be appreciated that while the periodicity was constant in the RTP1 sample with an estimated lattice parameter of 14.92 μm in average, determined after taking high magnification images of the sample, the periodicity of the RTP2 sample was sub-modulated into two different sub-periods of 9.5 and 10.5 μm approximately, inside of a longer period of 20 μm, imposed by the alternative grooves of the diffraction grating.

Micrographs of the samples were recorded in a FEI QUANTA 600 Scanning Electron Microscope (SEM) on top and lateral views to investigate the structure of the formed grooves at a local level. Fig. 3a and b shows top and lateral views, respectively, of the diffraction grating with $\Lambda = 15$ μm recorded by ultrafast laser ablation on the surface of the RTP1 sample. Fig. 3c and d shows two micrographs of the diffraction grating with $\Lambda = 20$ μm (with subperiods with lattices of 10.5 μm and 9.5 μm) recorded on the surface of RTP2 sample. The insets in Fig. 3a and c shows higher magnification images of the grating structures of RTP1 and RTP2 samples, respectively. From these micrographs we can still appreciate the high periodicity of the fabricated structures; however, the roughness of the lateral walls of the grooves was estimated to be 0.4 μm. This roughness can be a consequence of melting/vaporization and redeposition of material generated by the multipulse ablation processing, since each successive pulse would melt and vaporize the material and this would get redeposited in and around the groove, as observed in other dielectric materials [24]. Furthermore, the lateral views recorded for these two samples show that the grooves have a V shape with depths between $t = 5 \pm 0.4$ μm and $t = 7 \pm 0.4$ μm, and maximum widths of 5–5.5 μm for sample RTP1, and 3.3–3.5 μm for sample RTP2, respectively. Due to the low peak fluence used in the processing of these samples, we did not observe the formation of deposition of material at the edge of the groove, neither splattered material, as it happened with moderate peak fluences in $LiNbO_3$ [24].

These values are consistent with the fluence distribution (basically an Airy function) on the surface of the samples. In the case of RTP1, the region where the fluence exceeds the ablation threshold fluence (multishot conditions) has a width of approximately 5 ± 0.4 μm where as for RTP2 the corresponding width is 3.4 ± 0.4 μm. In both cases, the agreement with the width of the grooves is really good.

When we compare the results we obtained in RTP with those obtained in other non-linear optical materials, such as $LiNbO_3$ [24–26], $LiTaO_3$ [17] or BaB_2O_4 [16], we observed that for the wavelength and the processing conditions we used for the ablation process, similar features were observed in terms of roughness, however, deeper grooves were obtained at similar peak fluences in our case. When decreasing the peak fluence to values slightly above the ablation threshold, smoother features could be inscribed in $LiNbO_3$ [16,27], with a depth similar to those obtained in RTP, or submicrometer structures could be fabricated [26], still showing a high roughness, if the peak fluence is reduced to values close to the damage threshold.

It is well known that gratings of better quality and finer pitch can be fabricated using chemical etching techniques, becoming the standard techniques to fabricate such diffraction gratings in SiO_2 and many other materials, including $LiNbO_3$ [28].

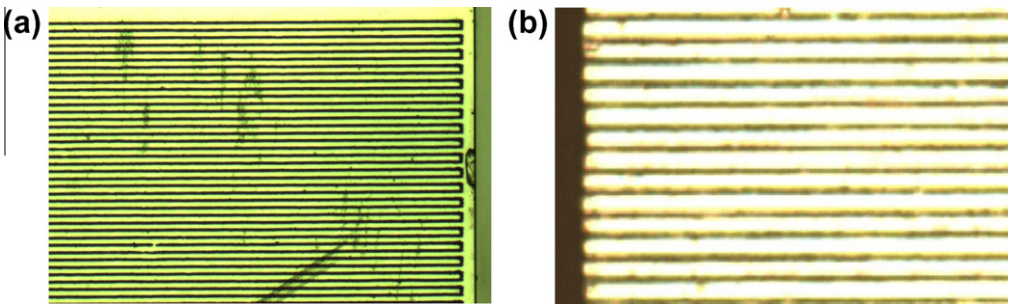

Fig. 2. Long range order optical microscope images of the RTP samples: (a) image taken with 5× objective and showing the regular pattern of the RTP 1 sample with a period of 15 μm and (b) image taken with 20× objective and showing the regular pattern of the RTP2 sample with a spatial period of 20 μm.

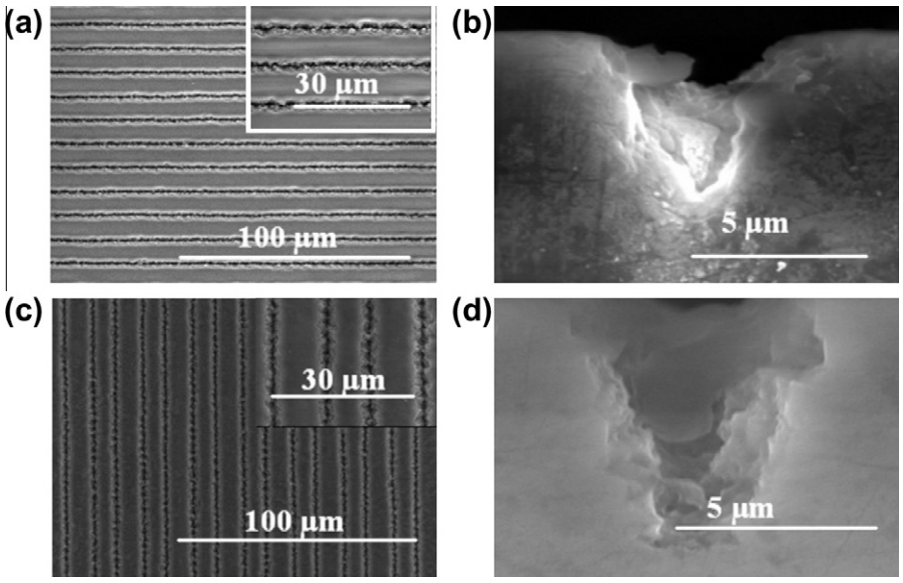

Fig. 3. SEM images recorded from the diffraction gratings fabricated by ultrafast laser ablation: (a) top view and (b) lateral view of the diffraction grating with a period of 15 μm recorded on the surface of the RTP1sample; (c) top view and (d) lateral view of the diffraction grating with a spatial period of 20 μm recorded on the surface of the RTP2 sample.

Thus, we explored the possibilities of using chemical etching to improve the quality of the diffraction gratings we fabricated on the surface of RTP by ultrafast laser ablation. Selective chemical etching in KTP and other crystals of the same family, including RTP, has been extensively studied to visualize the ferroelectric domain distribution in this family of materials [29]. This distribution of ferroelectric domains can be observed by etching the (001) face of these crystals with a mixture of KOH:KNO_3 2:1 M ratio at 353 K. Since the diffraction gratings were inscribed on the (001) face of RTP crystals we checked the possibility of using this etchant to smooth the grooves fabricated by ultrafast laser ablation.

Fig. 4 shows the results obtained in this process for the RTP2 sample using different etching times ranging from 5 min to 1 h, together with a high magnification of the as-fabricated grooves for comparison. We observed that the edge of the groove is better defined with the chemical etching and the roughness of the lateral walls of the channels is reduced. The best results were obtained for an etching time of 15 min. Beyond this etching time, the groove is becoming more and more wider when we increase the etching time, and even some of the parts of the sample not affected by the inital laser ablation process start to be affected after 1 h of exposure to the etchant. This would indicate that the sample was not single ferroelectric domain, and that for long exposure times we start to reveal the distribution of the ferroelectric domains on the surface of the sample. Also we observed that some trenches are formed at the lateral walls of the grooves by applying this etching technique. In any case, it is clear that chemical etching with KOH:KNO_3 can be used to improve the quality of the features fabricated on the (001) surface of RTP crystals by ultrafast laser ablation.

3.3. Determination of the lattice parameters of the diffraction gratings by FT-IR

Bragg-diffraction spectra of these samples have been recorded by using an FT-IR spectrometer (Bruker-Vertex 70) equipped with a special attachment that allows recording the spectra by reflectivity. We used a halogen tungsten lamp as the lighting source, and we collected the intensity of the diffracted light from 7500 to 400 cm^{-1} by using a DLATGS detector. The incoming light was pointed perpendicular to the surface of the sample where the 1D diffraction grating was recorded with the grooves perpendicular to the direction of the incident beam and several diffraction spectra were measured perpendicularly to the grooves at collection angles (θ) ranging from 24° to 60° in 2° steps. To evaluate the lattice constant, the Bragg-diffraction spectra were fitted to the 2-variable function:

$$I(\lambda, \sin\theta) \propto \sum_{n=1}^{3} \exp(-[(\sin\theta - (n\lambda/a))/w_n]^2) \quad (1)$$

where a is the lattice constant of the diffraction grating, n is the diffraction order, and w_n is a parameter that takes into account the width of diffraction peaks. By fitting this function to the experimental data we obtain a robust estimation of the lattice constant of the diffraction grating, since all measurements are taken into account simultaneously. Fig. 5a and b shows the 2D intensity plots as a function of the wavelength and the sinus of the diffraction angle of the measured data and the calculated data by the fitted function, respectively, for the diffraction grating recorded on the surface of the RTP1 sample. Experimentally, we observed three diffraction orders, that can be seen in the figure as dark red[1] color zones, with widths decreasing as the wavelength increased. The most intense peak was referred as the zero order peak and appeared in the range between 4 and 8 μm for low values of $\sin\theta$ with a lower slope. The second and third diffraction orders are observed at higher values of $\sin\theta$ with higher slopes.

The value of the lattice constant determined by this procedure was 14.98 μm for the diffraction grating recorded on the surface of RTP1 sample. This result is in good agreement with the value for the lattice constant for this sample estimated by optical and electron microscopy. For RTP2, using the same methodology, we were able to determine of the main periodicity, that was 19.85 μm. However, it has been impossible to determine the lattice constant of the two sub-periods existing in the RTP2 sample that we could observe only by optical and electronic microscopy.

[1] For interpretation of color in Figs. 1, 2, 5–10, the reader is referred to the web version of this article.

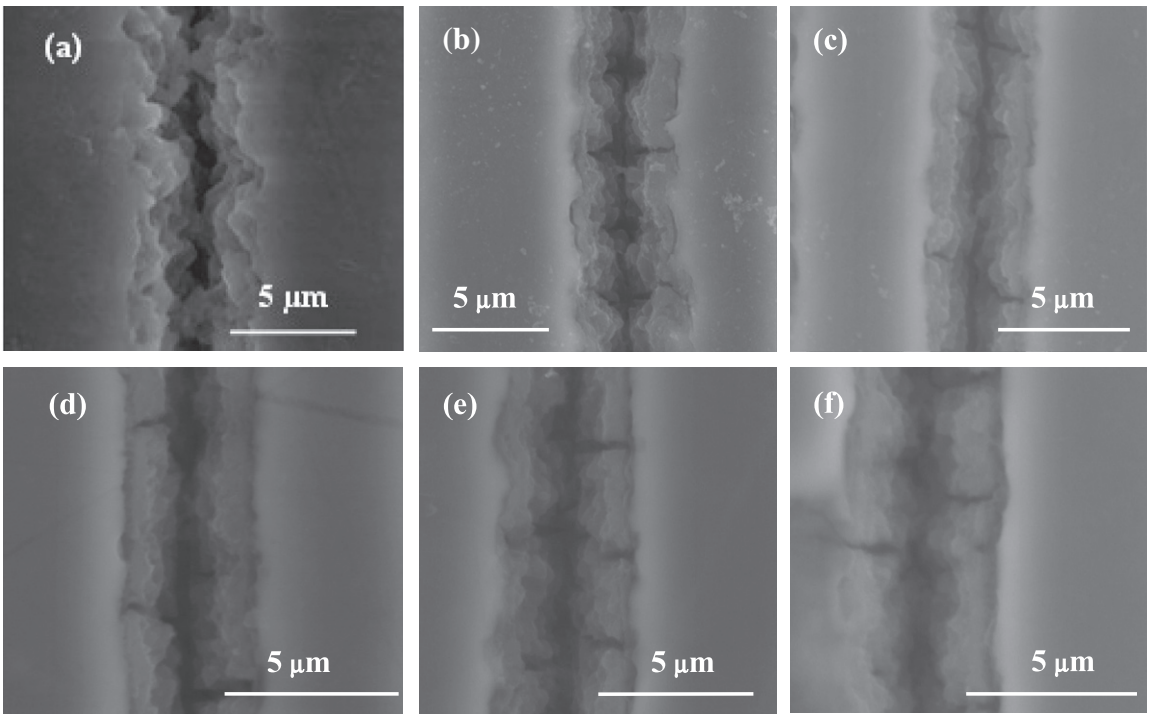

Fig. 4. SEM images of the grooves fabricated by ultrafast laser ablation after chemical attack with KOH:KNO_3 at different etching times: (a) 0 min, (b) 5 min, (c) 10 min, (d) 15 min, (e) 30 min, and (f) 1 h.

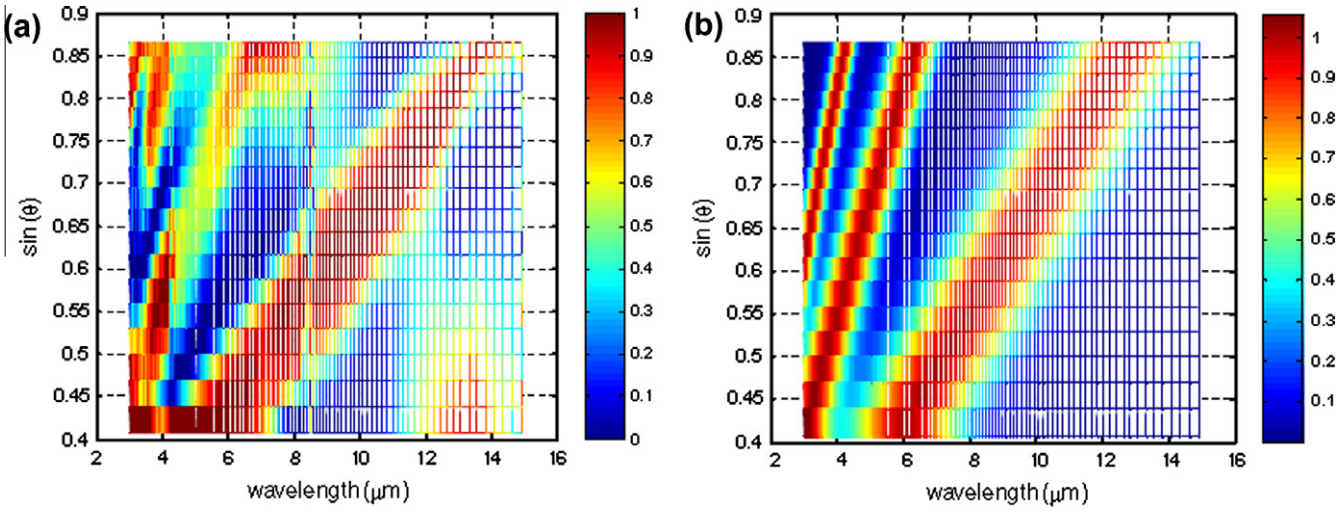

Fig. 5. (a) 2D experimental intensity plot as a function of the wavelength and the diffraction angle of the diffraction grating with a period of 15 μm recorded by ultra fast laser ablation on the surface of RTP1 sample: dark red zones represent the diffraction orders. (b) 2D plot of the fitted function to the experimental data after considering three diffraction orders.

3.4. Determination of the filling fraction of the diffraction gratings from the diffraction patterns

To check the quality of the diffraction gratings fabricated by these methods we recorded the linear diffraction patterns generated by the samples, obtained after focusing the beam of a He–Ne laser at 632.8 nm with a power of 3 mW and a spot size of ~1 mm on the surface of our samples, both in transmission and reflection geometries. In the transmission geometry the incident beam was set perpendicular to the surface of the sample on which the diffraction grating was inscribed, and the diffraction pattern was recorded at 180°. In the reflection geometry the incident beam was set to form an angle of 42° with the perpendicular to the surface of the diffraction grating to avoid additional spots on the diffraction patterns generated by internal reflections in other faces of the crystals. Fig. 6 shows the obtained diffraction patterns for the two samples analyzed.

On the screen, up to 11 diffraction orders, from −5 to +5, were visible in the transmission geometry for the RTP1 sample, while only 9 diffraction orders, from −4 to +4, were visible in the reflection geometry, as shown in Fig. 6a and b. In the RTP2 sample, even a larger number of spots could be observed, up to 15 diffraction orders, from −7 to +7, were visible in the transmission geometry, while this number was reduced to 11 diffraction orders, from −5 to +5, in the reflection geometry. Furthermore, the sub-modulation of the period of the diffraction grating is reflected in an alternation

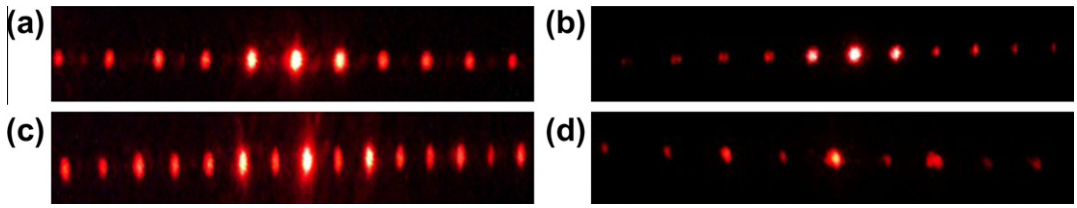

Fig. 6. Linear diffraction patterns of the different diffraction gratings recorded after illuminating the sample with a He–Ne laser: (a) diffraction grating with a period of 15 μm fabricated by ultrafast laser ablation on the surface of an RTP1 sample in transmission, and (b) in reflection geometries. (c) Diffraction grating with a spatial period 20 μm on the surface of RTP2 sample in transmission and (d) in reflection geometries.

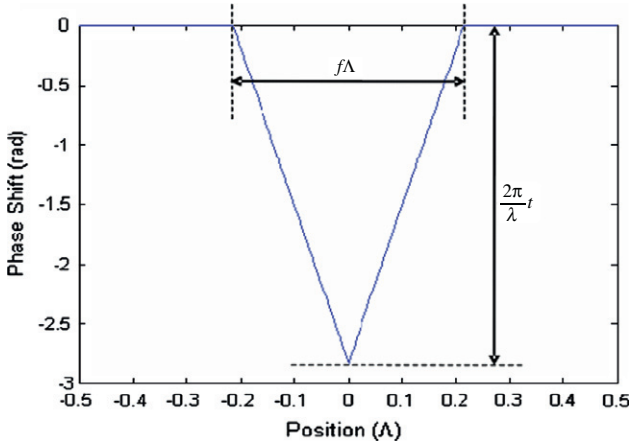

Fig. 7. Phase shift profile used to model the unit cell corresponding to the diffraction grating inscribed on the RTP1 sample, considered as a phase-only grating.

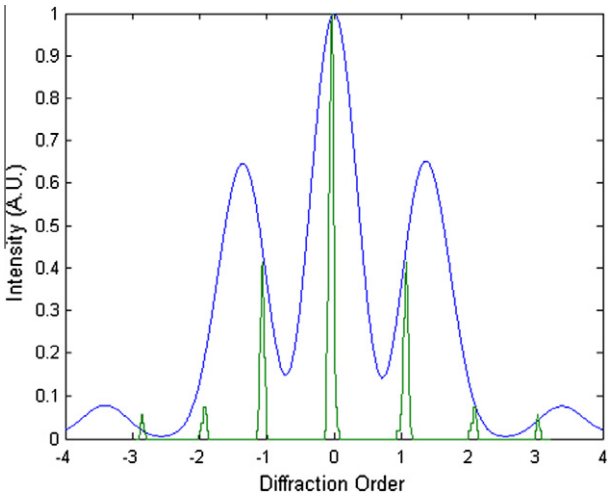

Fig. 8. Relative intensity profile of the diffraction pattern (green) and envelope profile (blue) for the RTP1 sample.

of high intensity and low intensity diffraction spots in the pattern as can be seen in Fig. 6c and d. Thus, in this way we demonstrate that these structures can work as both transmission and reflection gratings, fabricated within a single process.

The number of modes observed in these diffraction gratings are similar to those recorded previously in diffraction gratings inscribed in the surface of $LiNbO_3$ [14] and $BaBO_3$ [16] using the same methodology, indicating that the quality of the diffraction gratings in all those cases is similar.

We recorded the intensity profiles of the transmitted diffraction patterns with a charge coupled device (CCD) camera. Due to the limited dynamic range of the CCD camera we used, only the most intensity peaks of the diffraction patterns could be recorded. Diffraction patterns are sensitive to change in the periodicity of the grating or filling fraction. The filling fraction f is referred to as the fraction of the grating period that is filled with the grating material with values smaller than 1 (a value of 1 would mean that no diffraction grating exist on our sample). The analysis of the intensity profiles of the diffraction gratings can provide the characteristics of the fabricated diffraction gratings on the surface of the crystals, and can be used to determine from them the filling fraction.

In order to model the grooves with a V shape, the grating has been considered as a phase-only grating, where the grooves introduce a lower phase shift with respect to the parts of the grating without grooves. For RTP1, the phase shift profile of the unit cell is shown in Fig. 7. The position within the unit cell is expressed in terms of the lattice constant (Λ). In the figure, the different parameters describing the V-shaped grooves (f and t, where t defines the depth of the grooves) are indicated. The intensity profile of the diffraction grating on the RTP1 sample is shown in Fig. 8 together with the best fit of the experimental data, corresponding to a filling fraction $f = 0.43$ and a depth $t = 0.45\ \lambda$.

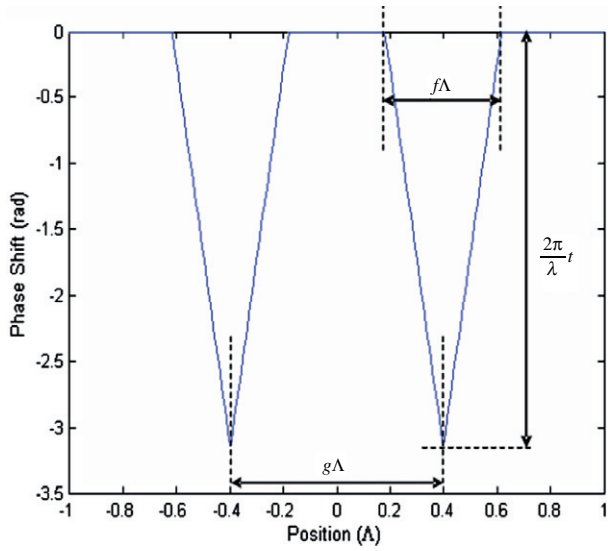

Fig. 9. Phase shift profile used to model the unit cell corresponding to the diffraction grating inscribed on the RTP2 sample, considered as a phase-only grating.

For RTP2, the profile considered to model our diffraction grating and the corresponding parameters are indicated in Fig. 9. This unit cell is periodically repeated every 2Λ. The experimental data together with the best fit are shown in Fig. 10. It is important to notice that in the case of the intensity profile of the RTP2 sample, the

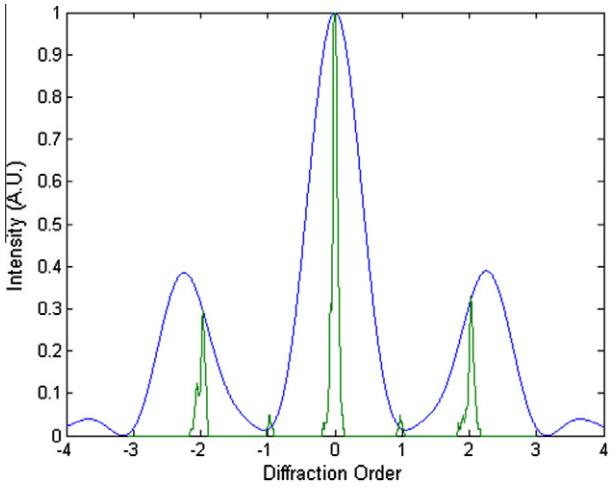

Fig. 10. Relative intensity profile of the diffraction pattern (green) and envelope profile (blue) for the RTP2 sample.

±1 order has lower intensity than the ±2 diffraction order peak. This variation in the intensity of diffraction orders were observed due to the existence of the 10.5 μm and 9.5 μm subperiodicities at the spatial period of 20 μm. The corresponding parameters for the best fit are $g = 0.92$, $f = 0.75$ and $t = 0.35\ \lambda$. The exact value for g should be 0.95, according to the subperiodicities observed in the sample. However, no reasonable fit could be obtained with this value of g, indicating also that these subperiodicities are not exact.

The profile of the envelope of the diffraction order maxima is the modulus square of the Fourier transform of the unit cell transmittance (unit amplitude and phase as indicated in Figs. 7 and 9), in the adequate scale. An analytic expression of this envelope should be very complex, difficult to obtain and very long to be included in the paper.

The diffraction efficiency for these samples was estimated by comparing the intensity recorded at the zero order with that of the incident beam. In both cases, this diffraction efficiency was found to be at around 0.1%. This value is not surprising since the measurements were not performed at the optimum wavelength for these diffraction gratings. However, comparing the quality of the diffraction gratings inscribed in RTP with those inscribed in $LiNbO_3$ for which up to a 30% diffraction efficiency has been reported [14] and those inscribed in $BaBO_3$ with diffraction efficiencies between 50% and 60% [16], one would expect to get similar values when using the optimum wavelength.

4. Conclusions

In conclusion, we have fabricated surface-relief diffraction gratings on ***c***-oriented RTP samples with different lattice constants by ultrafast laser ablation, and we characterized them morphologically and optically. The roughness observed on the surface of the channels of these diffraction gratings is similar to that observed previously in diffraction gratings fabricated on the surface of other non-linear optical materials, such as $LiNbO_3$, $LiTaO_3$ and $BaBO_3$ using the same methodology. However, the quality of the diffraction grating can be improved by using chemical etching techniques. A high number of diffraction orders were observed in the two samples analyzed, comparable to those recorded in diffraction gratings inscribed in $LiNbO_3$ and $BaBO_3$, indicating that the quality of the diffraction gratings inscribed in RTP is similar to those reported previously in other non-linear optical materials. It is obvious that the large edge roughness observed for these diffraction gratings inscribed by laser ablation on the surface of non-linear optical materials would make them more suitable for operation in the mid-infrared spectral range, were metallic rolled gratings can be fabricated in a simpler way, however, in those cases we can take advantage of the non-linear optical properties of the material to convert part of this radiation to the near-infrared or to the visible in the optimum cases.

We think that such surface-relief diffraction gratings may find potential applications in situations in which collinear phase matching configurations for SHG in non-linear optical materials cannot be achieved, such as signal multiplexing. This possibility will be analyzed in the future.

Acknowledgments

This work was partially funded by the European Commission under the Seventh Framework Program under Project Cleanspace FP7-SPACE-2010-1-GA-263044, supported by the Spanish Government under Projects PI09/90527, TEC2009-09551, AECID A/024560/09, FIS2009-09522, HOPE CSD2007-00007 and SAUUL CSD2007-00013 (Consolider-Ingenio 2010), by Catalan Government under Projects 2009SGR235 and 2009SGR549, by Junta de Castilla y León under Project GR27, and by the Research Center on Engineering of Materials and Systems (EMaS) of the URV. J.J.C. is supported by the Education and Science Ministry of Spain and European Social Fund under the Ramón y Cajal program, RYC2006-858. We also acknowledge support from the Centro de Laseres Pulsados, CLPU, Salamanca, Spain.

References

[1] J. Armstrong, N. Bloembergen, J. Ducuing, P.S. Pershan, Phys. Rev. 127 (1962) 1918.
[2] P.A. Franken, J.F. Ward, Rev. Mod. Phys. 35 (1963) 23.
[3] J. Martorell, R. Vilaseca, Phys. Rev. A 55 (1997) 4520.
[4] T.R. Zhang, H.R. Choo, M.C. Downer, Appl. Opt. 29 (1990) 3927.
[5] M.E. Hagerman, K.R. Poeppelmeier, Chem. Mater. 7 (1995) 602.
[6] M.N. Satyanarayana, A. Deepthy, H.L. Bhat, Crit. Rev. Solid State Mater. Sci. 24 (1999) 103.
[7] M. Roth, M. Tseitlin, N. Angert, Phys. Chem. 31 (2005) 86.
[8] D.N. Nikogosyan, Nonlinear Optical Crystals A Complete Survey, Springer, Berlin, 2005.
[9] A.R. Cowan, J.F. Young, Phys. Rev. B 65 (2002) 085106.
[10] R. Reinsch, M. Néviere, Phys. Rev. B 28 (1983) 1870.
[11] A.M. Malvezzi, F. Cattaneo, G. Vecchi, M. Falasconi, G. Guizzetti, L.C. Andreani, F. Romanato, L. Businaro, E. Di Fabrizio, A. Passaseo, M. De Vittorio, J. Opt. Soc. Am. B 19 (2002) 2122.
[12] M. Lenzner, J. Kruger, S. Sartania, Z. Cheng, Ch. Spielmann, G. Mourou, W. Kautek, F. Krausz, Phys. Rev. Lett. 80 (1998) 4076.
[13] C. Méndez, J.R. Vázquez de Aldana, G.A. Torchia, L. Roso, Opt. Lett. 30 (2005) 2763.
[14] G.A. Torchia, C. Méndez, I. Arias, L. Roso, A. Rodenas, D. Jaque, Appl. Phys. B 83 (2006) 559.
[15] C. Romero, J.R. Vázquez de Aldana, C. Méndez, L. Roso, Opt. Express 16 (2008) 18109.
[16] Y. Li, P. Lu, N. Dai, X. Wang, Y. Wang, b. Yu, H. Long, Appl. Phys. B 88 (2007) 227.
[17] Y. Zhang, X. Chen, H. Chen, Y. Xia, Appl. Surf. Sci. 253 (2007) 8874.
[18] J.J. Carvajal, C.F. Woensdregt, R. Solé, F. Díaz, M. Aguiló, Cryst. Growth. Des. 6 (2006) 2667.
[19] J.J. Carvajal, R. Solé, J. Gavaldà, J. Massons, M. Aguiló, F. Díaz, Opt. Mater. 24 (2003) 425.
[20] J.J. Carvajal, V. Nikolov, R. Solé, Jna. Gavaldà, J. Massons, M. Rico, C. Zaldo, M. Aguiló, F. Díaz, Chem. Mater. 12 (2000) 3171.
[21] G. Dumitru, V. Romano, H.P. Weber, M. Sentis, W. Marine, Appl. Phys. A 74 (2002) 729.
[22] K. Iliev, P. Peshev, V. Nikolov, I. Koseva, J. Cryst. Growth 100 (1990) 225.
[23] Jna. Gavaldà, J.J. Carvajal, X. Mateos, M. Aguiló, F. Díaz, Appl. Phys. Lett. 95 (2009) 182902.
[24] D.C. Deshpande, A.P. Malshe, E.A. Stach, V. Ramilovic, D. Alexander, D. Doerr, D. Hirt, J. Appl. Phys. 97 (2005) 074316.
[25] P. Galinetto, D. Ballarini, D. Grando, G. Samoggia, Appl. Surf. Sci. 248 (2005) 291.
[26] B. Yu, P. Lu, N. Dai, Y. Li, X. Wang, Y. Wang, Q. Zheng, J. Opt. A: Pure Appl. Opt. 10 (2008) 035301.

[27] A. Rodenas, J.A. Sanz García, D. Jaque, G.A. Torchia, C. Mendez, I. Arias, L. Roso, F. Agulló-Rueda, J. Appl. Phys. 100 (2006) 033521.
[28] J. Capmany, C.R. Fernandez-Pousa, E. Dieguez, V. Bermudez, Appl. Phys. Lett. 83 (2003) 5145.
[29] F. Laurell, M.G. Roelofs, W. Bindloss, H. Hsiung, A. Suna, J.D. Bierlein, J. Appl. Phys. 71 (1992) 4664.